

# An electromagnetic black hole made of metamaterials

Qiang Cheng and Tie Jun Cui\*

State Key Laboratory of Millimeter Waves, Department of Radio Engineering

Southeast University, Nanjing 210096, China.

\*To whom correspondence should be addressed.

E-mail: [tjcui@seu.edu.cn](mailto:tjcui@seu.edu.cn).

Traditionally, a black hole is a region of space with huge gravitational field in the means of general relativity, which absorbs everything hitting it including the light. In general relativity, the presence of matter-energy densities results in the motion of matter propagating in a curved spacetime<sup>1</sup>, which is similar to the electromagnetic-wave propagation in a curved space and in an inhomogeneous metamaterial<sup>2</sup>. Hence one can simulate the black hole using electromagnetic fields and metamaterials. In a recent theoretical work, an optical black hole has been proposed based on metamaterials, in which the numerical simulations showed a highly efficient light absorption<sup>3</sup>. Here we report the first experimental demonstration of electromagnetic black hole in the microwave frequencies. The proposed black hole is composed of non-resonant and resonant metamaterial structures, which can absorb electromagnetic waves efficiently coming from all directions due to the local control of electromagnetic fields. Hence the electromagnetic black hole could be used as the thermal emitting source and to harvest the solar light.

The concept of black hole appears in the general theory of relativity. The black hole actually represents a region of space in which the gravitational field is so powerful that everything including the light hitting it cannot escape. Similar to the perfect black body in the thermodynamics<sup>4</sup>, the black hole has a one-way surface. It absorbs all the light into the surface without any reflections, and hence nothing comes out from the black hole. In the general relativity, the presence of matter-energy densities results in the motion of matter and the light propagating in a curved space-time domain<sup>5</sup>. This behaviour is very similar to the light or electromagnetic-wave propagation in a curved space and in an inhomogeneous metamaterial. In fact, there exists an analogy between the mechanics and optics, which is revealed by the least-action principle for the motion of particle in mechanics and the Fermat principle for the propagation of light in optics<sup>5</sup>.

The optical-mechanical analogy provides a useful link between the light/electromagnetic-wave propagation in inhomogeneous media and the particle/light motion in gravitational potentials. Hence one can study the celestial phenomena such as photonic black holes by observing the photon motion in inhomogeneous metamaterials through numerical simulations<sup>5</sup>. In a recent theoretical work, another optical black hole has been proposed based on the metamaterials<sup>3</sup>. Theoretical analysis and numerical simulations have shown that the black hole can absorb the light waves in all directions and in a broad frequency band with highly efficiency<sup>3</sup>. However, the optical/photonic black holes based on metamaterials were only considered in theory and numerical simulations in the previous studies<sup>3,5</sup>, and the experimental verifications have not been reported.

During the past ten years, metamaterial has been a hot research topic in the scientific

community. The advances of artificial metamaterials in theories and experiments have offered scientists potent ways to tailor the properties of electromagnetic waves in the curvilinear space. Metamaterials have manifested a lot of exciting effects and devices, such as the negative refraction, electromagnetic invisibility cloaks, super-resolution imaging, electromagnetic concentrators, and light trapping<sup>6–22</sup>, in which the required constitutive parameters could be fulfilled by periodic/non-periodic arrays of electric or magnetic resonant/non-resonant particles. The current technologies for designing and fabricating metamaterials have enabled people to realize such functional devices with unusual electromagnetic properties.

In this work, we realize the electromagnetic black hole in the microwave frequencies based on the theoretical prediction to the optical black hole using non-magnetic metamaterials with broad-band omnidirectional light absorption<sup>3</sup>. We have designed and fabricated the microwave black hole using non-resonant and resonant metamaterial structures, and measured the internal electric fields using a planar-waveguide near-field scanning apparatus. Experimental results have good agreements to full-wave numerical simulations, which show obvious phenomena of microwave bending and trapping into the black hole. Hence the microwave black hole can absorb electromagnetic waves efficiently coming from all directions, which could find wide applications in the thermal emitting and the solar-light harvesting.

In the general relativity, the motion of matter/photon will be attracted to massive celestial object. In theory, the motion in the inherent spatial coordinates and universal time (the spacetime) can be described by the Hamilton equations:

$$\frac{d}{dt}p(t) = -\frac{\partial\mathcal{H}}{\partial q}, \quad \frac{d}{dt}q(t) = -\frac{\partial\mathcal{H}}{\partial p}, \quad (1)$$

in which  $p$  is the generalized momentum,  $q$  is the generalized coordinate, and  $\mathcal{H}$  is the Hamil-

tonian. The Hamiltonian represents the energy of the system, which is the sum of kinetic and potential energy, denoted by  $T$  and  $V$ , respectively, as  $\mathcal{H} = T + V$ ,  $T = p^2/(2m)$ ,  $V = V(q)$ , in which  $m$  is the mass of matter/photon.

From the electromagnetic theory, the scattering of dielectric objects has a similar Hamiltonian under the ray approximation<sup>3</sup>. In a two-dimensional (2D) isotropic non-magnetic dielectric cylinder with the following inhomogeneous electric permittivity

$$\epsilon(r) = \begin{cases} \epsilon_b, & r > R \\ \epsilon_s(r), & R_c \leq r \leq R, \\ \epsilon_c + i\gamma, & r < R_c \end{cases} \quad (2)$$

the Hamiltonian is given by<sup>3</sup>:  $\mathcal{H} = p_r^2/[2\epsilon(r)] + p_\theta^2/[2r^2\epsilon(r)]$ ,  $V(r) = \omega^2[\epsilon_b - \epsilon(r)]/(2C^2)$ , in which  $p_r$  and  $p_\theta$  are the radial and angular momentum,  $V$  is the central potential,  $c$  is the light speed, and  $\omega$  is the radian frequency. The theoretical analysis shows that the central potential  $V$  will be sufficiently attractive when  $\epsilon_s(r)$  satisfies  $\epsilon_s(r) = \epsilon_b(R/r)^2$ , which results in the electromagnetic rays falling onto the cylindrical center<sup>3</sup>. In such a case, the dielectric cylinder is equivalent to a 2D **black hole**, which could absorb nearly all incident electromagnetic rays.

As given in Eq. (2), the 2D black hole includes a lossy circular inner core, the payload, and a lossless circular shell with radially-varied electric permittivity, as shown in Fig. 1(a). Here,  $R_c$  and  $R$  stand for the radii of the inner core and outer shell of the black hole, while  $\epsilon_b$  and  $\epsilon_c$  represent the dielectric constants of the background medium and the lossy material inside the core. The radius of core is closely related to the ratio of two dielectric constants:  $R_c = R\sqrt{\epsilon_0/\epsilon_c}$ . Under the high-frequency (optical) approximation, it has been

proved that the scattering cross section per unit length of the black hole is nearly zero, which is independent of the polarization state of the incident waves<sup>3</sup>. Hence the black hole will absorb nearly all electromagnetic rays hitting on it from every direction, as illustrated in Fig. 1(a) for the ray-tracing approximation.

When the operating frequency falls into the microwave band, the high-frequency approximation will produce certain errors, which result in a small scattering cross section of the black hole. Hence we expect that the microwave black hole will absorb most electromagnetic waves incident to it from every direction with small scattering. Now we will validate the microwave black hole through numerical simulations and experiments. From Eq. (2), the permittivity distribution of the black hole's outer shell ( $R_c < r < R$ ) varies gradually from the inner core to the background medium. Thus the outer shell can be realized by gradient refraction index metamaterials, which have been used in the design of some new concept devices like the invisibility cloak<sup>11</sup> and the ground cloak<sup>13</sup>.

A number of non-resonant metallic structures could be utilized as the basic element of gradient refraction index metamaterials, such as the circular ring, the I-shaped structure, and the Jerusalem cross. The dimensions of unit geometries could be adjusted to meet the demand of refraction indices at specific positions, to achieve the gradient distribution. In non-resonant metamaterials, the resonant frequencies of unit geometries are much higher than the operating frequency, and the dispersion curves for effective permittivity and permeability change slowly in a broad band. Considering the anisotropy of most metamaterial unit, the electromagnetic constitutive parameters for the black hole are adjusted for the transverse-electric (TE) polarization in the cylindrical coordinate as  $\epsilon_z = \epsilon(r)$ ,  $\mu_\phi = 1$ , and  $\mu_r = 1$ . In

our design, we choose the non-resonant I-shaped structure<sup>13</sup> as the basic unit for the outer shell of the microwave black hole, and the electric-field-coupled (ELC) resonator<sup>21</sup> as the basic unit for the inner core, which has large permittivity and loss tangent simultaneously near the resonant frequency.

The photograph of fabricated microwave black hole is shown in Fig. 1(b), in which the I-shaped unit cell and ELC resonator are illustrated in Figs. 2(a) and 2(b), respectively. The black hole is placed in the air, hence the permittivity of the background medium is simply  $\epsilon_b = 1$ . In order to better demonstrate the absorption effect, a relatively high microwave frequency ( $f = 18$  GHz) is selected in simulations and experiments. The sizes of both I-shaped unit cell and ELC resonator are set as 1.8 mm, nearly 1/10 of the free-space wavelength. The whole black hole is composed of 60 concentric layers, and each layer is a thin printed circuit board (F4B,  $\epsilon = 2.65 + i0.001$ ) etched with a numbers of sub-wavelength unit structures on one side and coated with 0.018-mm-thick copper on the other side. From Eq. (2), the permittivity changes radially in the shell of black hole, and hence the unit cells are identical in each layer but have different sizes in adjacent layers. Since the permittivity is a constant in the lossy core, the ELC resonators are identical in the whole region.

Figure 2 demonstrates the effective medium parameters of the I-shaped and ELC units for the designed black hole. The full-wave numerical tool (Microwave Studio, CST2006b) has been used to simulate the electromagnetic properties. Following the standard retrieval procedure<sup>23</sup>, the effective permittivity and permeability are obtained from the S-scattering parameters with the change of geometry dimensions. To determine the relation between geometry and medium parameters, an interpolation algorithm has been developed to generate

the final layout according to the permittivity distribution required by the black hole. From Fig. 2(a), by changing the height of I-shaped unit, the real part of permittivity  $\text{Re}(\epsilon_z)$  ranges from 1.27 to 12.64 at 18 GHz, while the permeability components,  $\text{Re}(\mu_r)$  and  $\text{Re}(\mu_\phi)$ , are always close to unity. The imaginary parts of permittivity and permeability for the I-shaped unit, not shown here, are small enough to be neglected in the design of black hole. From Fig. 2(b), the operating frequency is near to the resonant frequency of the ELC structure, which results in a very lossy permittivity  $\epsilon_z = 9.20 + i2.65$  and lossy permeability components  $\mu_r = 0.68 - i0.01$  and  $\mu_\phi = 0.84 - i0.14$  at 18 GHz.

In our design, the spacing between adjacent layers is 1.8 mm, hence the radii of the black hole and the lossy core are determined immediately with  $R = 108$  mm and  $R_c = 36$  mm. There are totally 40 layers of the I-shaped structures and 20 layers of the ELC structures. In order to fix the 60 layers with different radii together, a 0.8-mm-thick styrofoam board has been used with 60 concentric circular slots carved by the LPKF milling machine (LKPF s100). Each layer has three unit cells in the vertical direction, and hence the height of black hole is 5.4 mm. To investigate the interactions between the fabricated black hole and incident TE-polarized electromagnetic waves, a parallel-plate waveguide near-field scanning system is used to map the field distributions near the black hole at 18 GHz. A similar apparatus has been discussed in Ref. 24. The separation between two plates is set as 6.5 mm, which is larger than the height of black hole to avoid the unnecessary dragging during measurements. The cutoff frequency of the waveguide system for the dominant TEM mode is 23 GHz. The bottom plate is mounted on a step motor which can translate in two dimensions. A monopole probe is fixed inside the waveguide as the feeding source, and a

corner reflector is placed on the back of source to produce the desired narrow beam. Four detection probes are placed on the top plate to measure the field distributions on a plane above the black hole under test, and each probe can scan a region of 200 mm by 200 mm independently. Hence the total scanning region is 400 mm by 400 mm with a step resolution of 0.5 mm. All probes are connected to a microwave switch which controls the measurement sequence after each movement of the step motors below the bottom plate. The two ports of a vector network analyzer (Agilent PNA-L N5230C) is connected to the feeding probe and the microwave switch respectively via cables. Then the measurement data are sent to the controlling computer for post processing.

In our experiments, two cases are considered when the electromagnetic waves are incident vertically and obliquely to the black hole. As a comparison, the full-wave numerical simulations are also given to illustrate the absorption effect. Figures 3(a) and (b) illustrate the distributions of simulated and measured electric fields  $|E_z|$  at 18 GHz for the vertical-incidence case, which agree to each other very well. It is clear that the incident beam becomes convergent inside the shell region and then enters the lossy core of black hole instead of being divergent in the free-space radiation. Different from the nearly perfect absorption to light waves in the optical black hole<sup>3</sup>, there exists small scattering besides the main absorption in the microwave black hole. When the beam is incident to the black hole at an oblique angle  $25^\circ$ , the waves are bent toward the central area and travel around the shell with distinct absorption, as demonstrated in Figs. 3(c) and (d). Clearly, the black hole is a good attractor to microwaves. Again, the simulation and experiment results have good agreements.

Comparing the experiment and simulation results with the theoretical prediction in the

optical frequency<sup>3</sup>, it is clear that the design for optical black hole still holds in the microwave region, except that the perfect absorption condition cannot be satisfied due to the small scattering. Hence we realize the electromagnetic black hole experimentally in the microwave frequency. When the operating frequency increases, more and more electromagnetic waves and energies are absorbed by the black hole. Figure 4(a) illustrates the electric field distributions inside and outside the black hole under the incidence of a higher-frequency beam at 50 GHz through full-wave simulations. Comparing with Fig. 3(c), we obviously notice that more waves are attracted by the black hole with better absorption of electromagnetic energy. The symmetrical geometry of the black hole makes it possible to absorb electromagnetic energies efficiently in all directions. Figure 4(b), (c), and (d) demonstrate the simulation results of electric fields when two, three, and eight beams are incident to the black hole obliquely and vertically at the frequency of 50 GHz. It is clear that all-direction incident beams are mostly attracted by the microwave black hole.

In summary, we have designed, fabricated, and measured an electromagnetic black hole at the microwave frequency using non-resonant I-shaped metamaterial and resonant ELC metamaterial structures based on the theoretical study<sup>3</sup>. We have observed that most of incident waves and energies are attracted by the designed black hole. The good consistence between theoretical and experimental results have shown the excellent ability for metamaterials as the candidate to construct the artificial black holes. We expect that the microwave black hole could find important applications in the solar-light harvesting, the thermal emitting, and the cross-talk reduction in microwave circuits and devices. The specially designed microwave black holes could also be used to control, slow, and trap the electromagnetic

waves, and to investigate more physics on the celestial mechanics.

## References

- [1] Kox, A. J. et al. (eds). *The Collected Papers of Albert Einstein*. Vol. 6 (Princeton Univ. Press, 1997).
- [2] Pendry, J. B., Schurig, D. & Smith, D. R. Controlling electromagnetic fields. *Science* **312**, 1780-1782 (2006).
- [3] Narimanov, E. E., Kildishev, A. V. Optical black hole: Broadband omnidirectional light absorber. *Appl. Phys. Lett.* **95**, 041106 (2009).
- [4] Davies, P. C. W. Thermodynamics of Black Holes. *Rep. Prog. Phys.* **41**, 1313 (1978).
- [5] Genov, D. A., Zhang, S., Zhang, X. Mimicking celestial mechanics in metamaterials. *Nature Phys.* (2009).
- [6] Smith, D. R., Padilla, W. J., Vier, D. C., Nemat-Nasser, S. C. & Schultz, S. Composite medium with simultaneously negative permeability and permittivity. *Phys. Rev. Lett.* **84**, 4184-4187 (2000).
- [7] Smith, D. R., Pendry, J. B. & Wiltshire, M. C. K. Metamaterials and negative refractive index. *Science* **305**, 788-792 (2004).
- [8] Zhang, X. & Liu, Z. W. Superlenses to overcome the diffraction limit. *Nature Mater.* **7**, 435-441 (2008).
- [9] Sarychev, A. K. & Shalaev, V. M. *Electrodynamics of Metamaterials* (World Scientific, 2007).

- [10] Soukoulis, C. M., Linden, S. & Wegener, M. Negative refractive index at optical wavelengths. *Science* **315**, 47-49 (2007).
- [11] Schurig, D. *et al.* Metamaterial electromagnetic cloak at microwave frequencies. *Science* **314**, 977-980 (2006).
- [12] Leonhardt, U. Optical conformal mapping. *Science* **312**, 1777-1780 (2006).
- [13] Liu, R., Ji, C., Mock, J. J., Chin, J. Y., Cui, T. J., Smith, D. R. Broadband ground-plane cloak. *Science* **323**, 366-369 (2009).
- [14] Valentine, J., Li, J., Zentgraf, T., Bartal, G. & Zhang, X. An optical cloak made of dielectrics. *Nature Mater.* **8**, 568-571 (2009).
- [15] Cai, W. S., Chettiar, U. K., Kildishev, A. V. & Shalaev, V. M. Optical cloaking with metamaterials. *Nature Photon.* **1**, 224-227 (2007).
- [16] Tyc, T. & Leonhardt, U. Transmutation of singularities in optical instruments. *New J. Phys.* **10**, 115038 (2008).
- [17] Leonhardt, U. & Tyc, T. Broadband invisibility by non-euclidean cloaking. *Science* **323**, 110-112 (2009).
- [18] Greenleaf, A., Kurylev, Y., Lassas, M. & Uhlmann, G. Electromagnetic wormholes and virtual magnetic monopoles from metamaterials. *Phys. Rev. Lett.* **99**, 183901 (2007).
- [19] Ma, G. M., C. K. Ong, Tyc, T. & Leonhardt, U. An omnidirectional retroreflector based on the transmutation of dielectric singularities. *Nature Mater.* **8**, 639-642 (2009).

- [20] Jiang, W. X., Cui, T. J., Cheng, Q., Chin, J. Y., Yang, X. M., Liu, R., Smith, D. R. Design of arbitrarily shaped concentrators based on conformally optical transformation of nonuniform rational B-spline surfaces. *Appl. Phys. Lett.* **92**, 264101 (2008).
- [21] Schurig, D, Mock, J. J. & Smith, D. R. Electric-field-coupled resonators for negative permittivity metamaterials. *Appl. Phys. Lett.* **88**, 041109 (2006).
- [22] Tsakmakidis, K. L., Boardman, A. D., & Hess, A. ‘Trapped rainbow’ storage of light in metamaterials. *Nature* **450**, 397-401 (2007).
- [23] Smith, D. R., Schultz, S. , Markos, P. & Soukoulis, C. M. Determination of effective permittivity and permeability of metamaterials from refraction and transmission coefficients. *Phys. Rev. B*, **65**, 195104 (2002).
- [24] Justice, B. J. *et al.* Spatial mapping of the internal and external electromagnetic fields of negative index metamaterials. *Opt. Express*, **14**, 8694 (2006).

## **Acknowledgement**

This work was supported in part by the National Science Foundation of China under Grant Nos. 60990320, 60990324, 60671015, 60496317, and 60901011, in part by the Natural Science Foundation of Jiangsu Province under Grant No. BK2008031, and in part by the 111 Project under Grant No. 111-2-05.

## **Author contributions**

Q. Cheng and T. J. Cui made contributions to the numerical simulations, the device design and implementation, and the experiments.

## List of Figure Captions

**Fig. 1:** (color online) (a) A model of black hole composed of a gradient-index metamaterial shell and a lossy dielectric core. (b) Photograph of the fabricated artificial black hole based on metamaterials, which is composed of 60 concentric layers, with the ELC structures in the core layers and the I-shaped structures in the shell layers.

**Fig. 2:** (color online) **a-b** Effective medium parameters for unit cells of the artificial black hole. (a) The relation between the effective permittivity (real part of  $\epsilon_z$ ) and permeability (real parts of  $\mu_r$  and  $\mu_\phi$ ) and the geometry dimension  $m$  for the I-shaped unit. The inset shows the sketch of the I-shaped unit, with  $w = 0.15$  mm and  $q = 1.1m$ . (b) The effective permittivity (real and imaginary parts of  $\epsilon_z$ ) and permeability (real parts of  $\mu_r$  and  $\mu_\phi$ ) versus to the frequency for the ELC resonator. The inset shows the sketch of the ELC unit, where  $t = 1.6$  mm,  $g = 0.3$  mm,  $p = 0.15$  mm, and  $s = 0.65$  mm.

**Fig. 3:** (color online) **a-d** Distributions of electric fields  $|E_z|$  for the designed black hole at the frequency of 18 GHz. An electric monopole is placed inside a corner reflector to produce the desired incident beam with finite width. The two circles stand for boundaries of the outer shell and the inner core. (a) The full-wave simulation result when the beam is vertically incident to the black hole. (b) The experiment result when the beam is vertically incident to the black hole. (c) The full-wave simulation result when the beam is obliquely incident to the black hole. (d) The experiment result when the beam is obliquely incident to the black hole.

**Fig. 4:** (color online) **a-d** Distributions of electric fields  $|E_z|$  for the microwave black hole at the frequency of 50 GHz based on full-wave simulations. (a) Single beam with oblique incidence. (b) Double beams with oblique incidence. (c) Triple beams with oblique incidence. (d) Eight beams with vertical incidence.

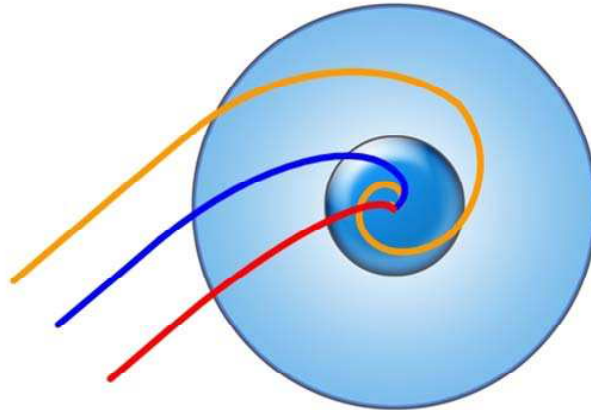
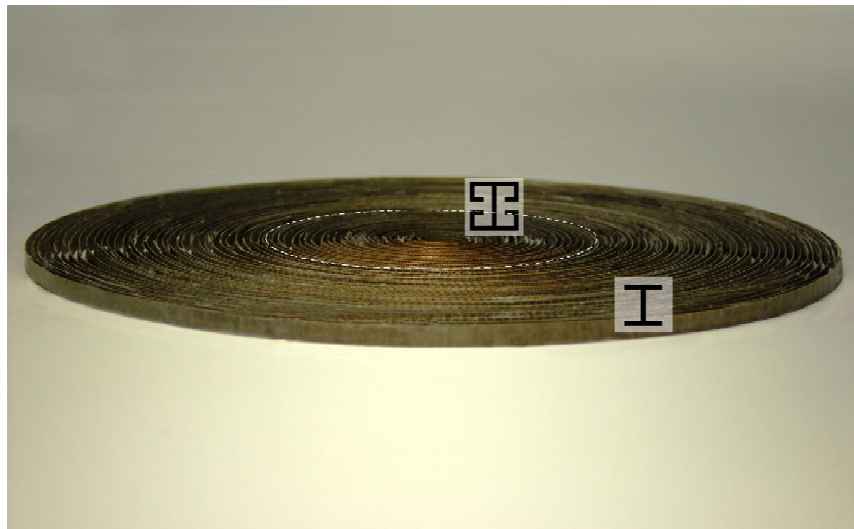
**a****b**

Figure 1: | (a) A model of black hole composed of a gradient-index metamaterial shell and a lossy dielectric core. (b) Photograph of the fabricated artificial black hole based on metamaterials, which is composed of 60 concentric layers, with the ELC structures in the core layers and the I-shaped structures in the shell layers.

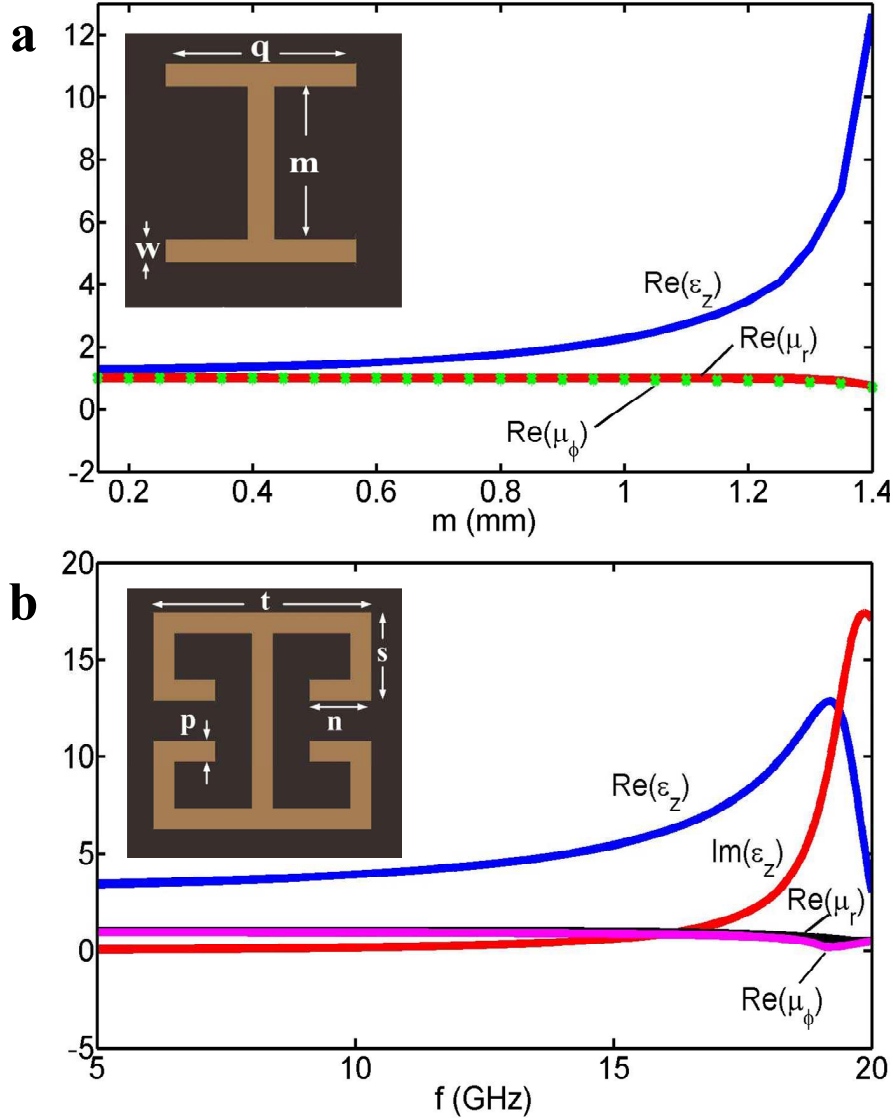


Figure 2: | **a-b** Effective medium parameters for unit cells of the artificial black hole. (a) The relation between the effective permittivity (real part of  $\epsilon_z$ ) and permeability (real parts of  $\mu_r$  and  $\mu_\phi$ ) and the geometry dimension  $m$  for the I-shaped unit. The inset shows the sketch of the I-shaped unit, with  $w = 0.15$  mm and  $q = 1.1m$ . (b) The effective permittivity (real and imaginary parts of  $\epsilon_z$ ) and permeability (real parts of  $\mu_r$  and  $\mu_\phi$ ) versus to the frequency for the ELC resonator. The inset shows the sketch of the ELC unit, where  $t = 1.6$  mm,  $g = 0.3$  mm,  $p = 0.15$  mm, and  $s = 0.65$  mm.

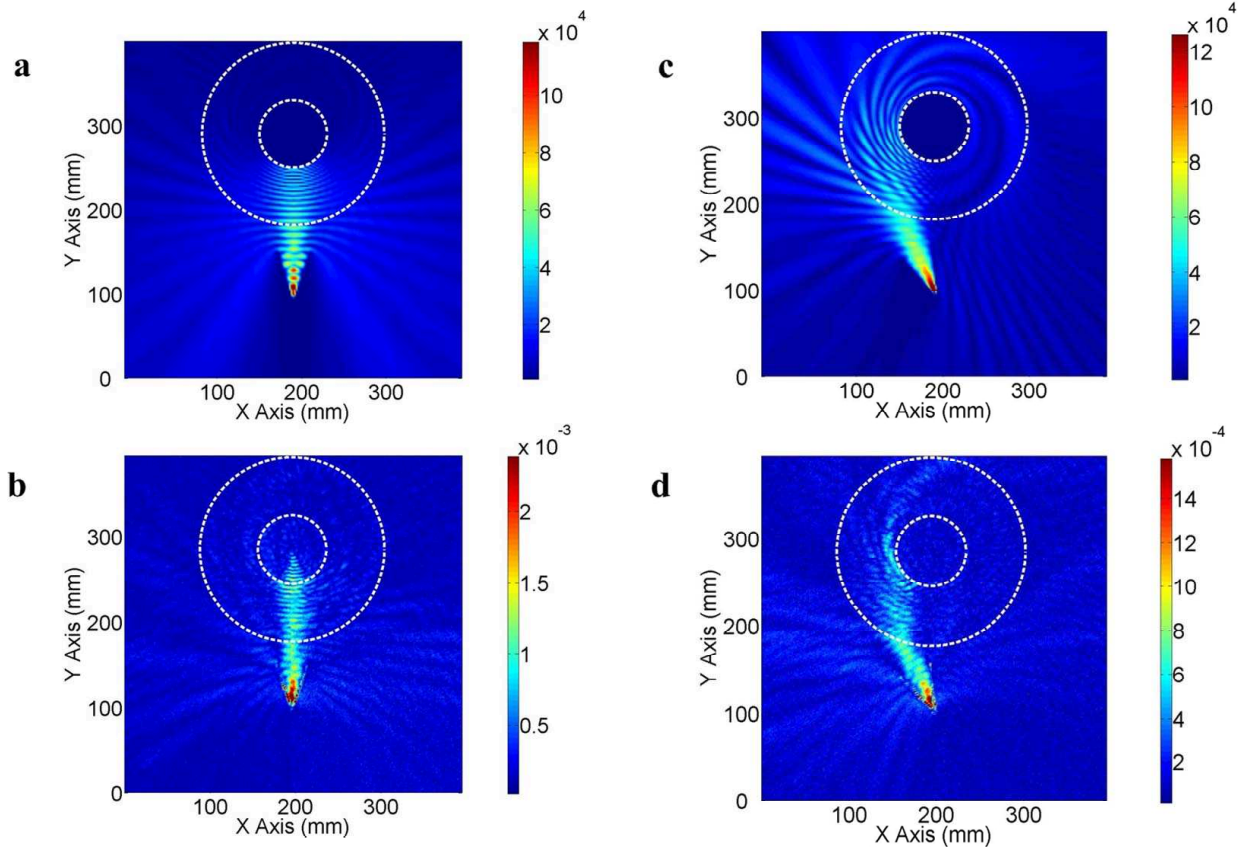


Figure 3: | **a-d** Distributions of electric fields  $|E_z|$  for the designed black hole at the frequency of 18 GHz. An electric monopole is placed inside a corner reflector to produce the desired incident beam with finite width. The two circles stand for boundaries of the outer shell and the inner core. (a) The full-wave simulation result when the beam is vertically incident to the black hole. (b) The experiment result when the beam is vertically incident to the black hole. (c) The full-wave simulation result when the beam is obliquely incident to the black hole. (d) The experiment result when the beam is obliquely incident to the black hole.

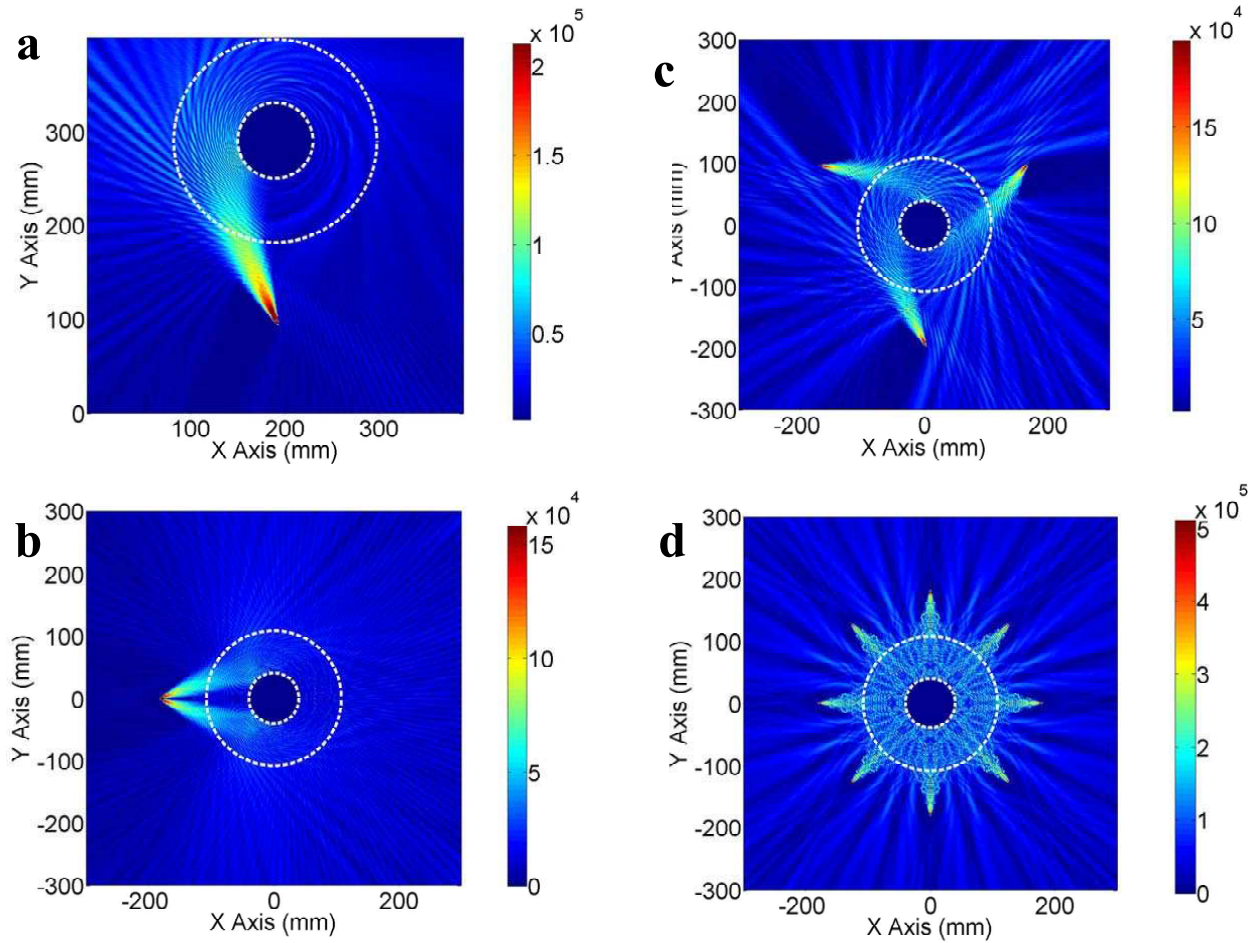


Figure 4: | **a-d** Distributions of electric fields  $|E_z|$  for the microwave black hole at the frequency of 50 GHz based on full-wave simulations. (a) Single beam with oblique incidence. (b) Double beams with oblique incidence. (c) Triple beams with oblique incidence. (d) Eight beams with vertical incidence.